Mon. Not. R. Astron. Soc. **375,** 77–91 (2007) doi:10.1111/j.1365-2966.2006.11111.x

# Radio signature of cosmological structure formation shocks

Matthias Hoeft⋆ and Marcus Brüggen⋆
*International University Bremen, Campus Ring 1, 28759 Bremen, Germany*

Accepted 2006 September 26. Received 2006 September 26; in original form 2006 June 27

**ABSTRACT**

In the course of the formation of cosmological structures, large shock waves are generated in the intracluster medium (ICM). In analogy to processes in supernova remnants, these shock waves may generate a significant population of relativistic electrons which, in turn, produce observable synchrotron emission. The extended radio relics found at the periphery of several clusters and possibly also a fraction of radio halo emission may have this origin. Here, we derive an analytic expression for (i) the total radio power in the downstream region of a cosmological shock wave, and (ii) the width of the radio-emitting region. These expressions predict a spectral slope close to −1 for strong shocks. Moderate shocks, such as those produced in mergers between clusters of galaxies, lead to a somewhat steeper spectrum. Moreover, we predict an upper limit for the radio power of cosmological shocks. Comparing our results to the radio relics in Abell 115, 2256 and 3667, we conclude that the magnetic field in these relics is typically at a level of 0.1 μG. Magnetic fields in the ICM are presumably generated by the shocks themselves; this allows us to calculate the radio emission as a function of the cluster temperature. The resulting emissions agree very well with the radio power–temperature relation found for cluster haloes. Finally, we show that cosmic accretion shocks generate less radio emission than merger shock waves. The latter may, however, be detected with upcoming radio telescopes.

**Key words:** radiation mechanisms: non-thermal – methods: analytical – galaxies: clusters: general – diffuse radiation – radio continuum: general.

## 1 INTRODUCTION

Diffuse radio objects that extend over several Mpc but have no optical counterpart have been observed in several clusters of galaxies. These objects fall into two categories: radio haloes are centrally located in the cluster; they are fairly regular in shape and show very little polarization. In contrast, radio relics appear at the periphery of clusters, have a filamentary morphology and are often highly polarized. Abell 3667, for instance, shows a spectacular double relic (Röttgering et al. 1997), where the two radio objects, separated by ∼4 Mpc, symmetrically straddle the cluster X-ray emission. Similarly, extended and remote relics have also been found in Abell 115 (Govoni et al. 2001b), Abell 2256 (Giovannini, Tordi & Feretti 1999), and Abell 2345 (Giovannini et al. 1999) to name just a few. All these clusters also show signs of an ongoing or recent merger: Abell 115 has a double peak in the centre in X-ray observations (Shibata et al. 1999), Abell 2256 shows also a double peak (Sun et al. 2002), Abell 2345 is assumed to be a dynamically young system since it shows multiple X-ray substructures (see discussion in Dahle et al. 2002), and in Abell 3667, among other indications, a cold front has been found which is presumably related to a slightly supersonically moving substructure (Vikhlinin & Markevitch 2002). In particular, the last example suggests that the relics are located at the shock wave that has been produced by the substructure. Roettiger, Burns & Stone (1999) were able to reproduce the X-ray morphology and the location of the radio emission for this particular cluster in a merger simulation.

Even if the X-ray emission at the periphery of galaxy clusters is too faint to identify clearly shock fronts, radio relics seem to trace cosmological shock waves. Two models have been proposed for the origin of radio relics: either they could be caused by diffusive shock acceleration of electrons at the shock waves themselves (Enßlin et al. 1998; Miniati et al. 2001), or they could be old radio bubbles that are compressed by the passing shock wave and thus induced to emit observable synchrotron emission again (Enßlin & Gopal-Krishna 2001; Enßlin & Brüggen 2002; Hoeft, Brüggen & Yepes 2004). The former relics are sometimes called *radio gischt*, while the latter ones are known as *radio phoenix* (Kempner et al. 2004). The radio relic in Abell 85 (Slee et al. 2001) may serve due to its size, morphology, and strong polarization as prototype for the radio phoenix class.

⋆E-mail: m.hoeft@iu-bremen.de (MH); m.brueggen@iu-bremen.de (MB)

© 2007 The Authors. Journal compilation © 2007 RAS

Downloaded from https://academic.oup.com/mnras/article/375/1/77/986307 by guest on 16 August 2022

Radio haloes, in contrast, do not directly trace the shock fronts. Instead, the radio morphology is similar to the overall X-ray morphology of the cluster (Govoni et al. 2001a). The radio spectrum of haloes tends to steepen with radius (Feretti et al. 2004, 2005). This may be regarded as an evidence for the fact that the emitting electrons are accelerated by turbulence in the ICM (Brunetti 2004), which is a result of a merger. However, the origin of the haloes is still unclear. There is increasing evidence that haloes are indeed related to cluster mergers, but it is a subject of a debate whether the relativistic electron population that is responsible for the radio emission is emitted by a central active galactic nucleus, whether it is produced by strong shocks, whether it stems from the decay of relativistic protons or whether it is generated by turbulence in the downstream region of the shocks (for a review see e.g. Feretti 2005). Interestingly, the radio power of haloes scales with the cluster X-ray luminosity (Feretti 2005) or, equivalently, with its temperature (Keshet, Waxman & Loeb 2004). Therefore, the non-thermal component in a galaxy cluster, if existent, seems to be related to the thermal plasma.

Numerical simulations show that the formation of the large-scale structures leads to a variety of shocks in the intracluster medium (ICM) and intergalactic medium (Miniati et al. 2000; Hoeft et al., in preparation; Pfrommer et al. 2006). These shocks are crucial for the thermal state of the ICM. As matter falls into the deep potential wells of galaxy clusters, its shocks lead to the high temperature of the ICM of $\sim 10^7$–$10^8$ K. Ryu et al. (2003) distinguished between 'internal' and 'external' shocks. The former affect material that is already heated to roughly the cluster temperature, whereas the latter heat rather cold gas for the first time. Hence, internal shocks are typically weak while external shocks are very strong.

Cosmic rays with energies up to $\sim 10^{15}$ eV are presumably accelerated at the shock fronts of supernova remnants (e.g. Berezhko, Ksenofontov & Völk 2003; Vink & Laming 2003). The acceleration is believed to be caused by diffuse shock acceleration (DSA): particles may be scattered repeatedly between the upstream and downstream regions, separated by the shock. Each time the particle crosses the front, it gains kinetic energy (see for a review Axford, Leer & Skadron 1978; Bell 1978a,b; Blandford & Ostriker 1978). Even though the physical conditions of shock waves in the ICM are somewhat different from those in supernova remnants, one would also expect DSA to be efficient at cosmological shocks.

Various groups have tried to estimate the radio emission of the shock fronts by combining the probability distribution of cosmic shock fronts with models for DSA and the subsequent synchrotron emission. Keshet et al. (2004) found that 10 per cent of the extragalactic radio background below 500 MHz should be caused by cosmic structure formation shocks for a $\Lambda$ cold dark matter cosmology. They assumed that the emission comes mainly from external accretion shocks, in particular those that surround massive clusters of galaxies. Essential for the radio emission is the strength of the magnetic field since the emission is synchrotron emission. Unfortunately, the magnetic field distribution in clusters of galaxies and their surroundings is difficult to determine and still poorly constrained (for a review see Govoni & Feretti 2004).

In this paper, we compute the radio emission in the downstream region of a shock front. We assume that DSA produces a relativistic electron population with a power-law distribution in the energy spectrum (Section 2.2). As the plasma moves downstream, the high-energy electrons cool by inverse-Compton (IC) and synchrotron losses (Section 2.3). The main objective of this paper is to derive an analytic expression for (i) the total radio power in the downstream region of a cosmological shock wave, and (ii) the width of the radio-emitting region. In particular, we wish to explore the dependence of the power, spectral shape and spatial extent of the radio emission on the magnetic field and the shock parameters.

We apply our model to the relics observed in Abell 115, 2256 and 3667 and infer the magnetic field strength in the relic region (Section 3). Assuming that the magnetic field energy density is a fixed fraction of the thermal energy allows us to express the radio power as a function of the cluster temperature (Section 4). Finally, we make predictions for the radio emission of cosmic accretion shocks (Section 5).

## 2 RADIO EMISSION BY NON-RADIATIVE SHOCKS

### 2.1 Non-radiative shocks

A shock surface separates two regions: the upstream plasma moves with a velocity $v_\mathrm{u}$ towards the shock front, while the downstream plasma departs with a velocity $v_\mathrm{d}$. As the plasma passes through the shock front, mass, momentum, and energy fluxes are conserved, which is expressed in the Rankine–Hugoniot relations:

$$\begin{aligned} \rho_\mathrm{u} v_\mathrm{u} &= \rho_\mathrm{d} v_\mathrm{d}, \\ P_\mathrm{u} + \rho_\mathrm{u} v_\mathrm{u}^2 &= P_\mathrm{d} + \rho_\mathrm{d} v_\mathrm{d}^2, \\ \frac{1}{2} v_\mathrm{u}^2 + u_\mathrm{u} + \frac{P_\mathrm{u}}{\rho_\mathrm{u}} &= \frac{1}{2} v_\mathrm{d}^2 + u_\mathrm{d} + \frac{P_\mathrm{d}}{\rho_\mathrm{d}}, \end{aligned} \tag{1}$$

where $\rho$ denotes mass density, $P$ pressure, and $u$ specific internal energy. On time-scales relevant for the shock propagation, we assume that the ICM behaves like a polytropic, ideal gas. Hence, the pressure can be written as

$$P = (\gamma - 1)\, \rho u, \tag{2}$$

where $\gamma$ is the adiabatic index, and the specific internal energy depends only on the gas temperature, $T$,

$$(\gamma - 1) \mu m_\mathrm{p}\, u = k_\mathrm{B} T, \tag{3}$$

where $m_\mathrm{p}$ is the proton mass and $\mu$ is the molecular weight. We determine the latter by adopting a fully ionized plasma with primordial chemical composition. In contrast to the conserved properties, the entropy of the plasma is increased by the dissipation at the shock front. For



Downloaded from https://academic.oup.com/mnras/article/375/1/77/986307 by guest on 16 August 2022

simplicity, the term 'entropy' will refer throughout this paper to a monotonic function of it, namely the entropic index,

$$S \equiv u\rho^{1-\gamma}. \tag{4}$$

The strength of non-radiative shocks in a polytropic gas can be characterized by a single parameter, for example, the compression ratio

$$r \equiv \frac{\rho_{\rm d}}{\rho_{\rm u}}, \tag{5}$$

or, equivalently, by the entropy ratio

$$q \equiv \frac{S_{\rm d}}{S_{\rm u}}. \tag{6}$$

The ratio of the specific internal energies can be given as a function of the compression and entropy ratios

$$\frac{u_{\rm d}}{u_{\rm u}} = \frac{S_{\rm d}}{S_{\rm u}} \left(\frac{\rho_{\rm d}}{\rho_{\rm u}}\right)^{\gamma-1} = qr^{\gamma-1}. \tag{7}$$

Combining the conservation laws, equation (2), and using the definition of the entropy, equation (4), allows us to relate the compression and the entropy ratios by the implicit equation

$$r = \frac{(\gamma+1)\,q\,r^{\gamma} + (\gamma-1)}{(\gamma-1)\,q\,r^{\gamma} + (\gamma+1)}. \tag{8}$$

Hence, if we can determine the entropy ratio, $q$, for a shock, we can compute the compression ratio by equation (8) and finally the ratio of internal energies by equation (7).

Customarily, the strength of a shock is characterized by the upstream Mach number

$$\mathcal{M} = \frac{v_{\rm u}}{c_{\rm u}}, \tag{9}$$

where $c_{\rm u}$ denotes the upstream sound speed, which depends on the specific internal energy by

$$c_{\rm u}^2 = \gamma(\gamma-1)\,u_{\rm u}. \tag{10}$$

Invoking flux conservation, equation (2), we can rewrite the Mach number

$$\mathcal{M}^2 = \frac{1}{c_{\rm u}^2}\,\frac{\rho_{\rm d}}{\rho_{\rm u}}\,\frac{P_{\rm d}-P_{\rm u}}{\rho_{\rm d}-\rho_{\rm u}} = \frac{r}{\gamma}\,\frac{qr^{\gamma}-1}{r-1}. \tag{11}$$

For large Mach numbers, the entropy ratio is proportional to $\mathcal{M}^2$ (Fig. 1). For later use, we rewrite the downstream velocity

$$v_{\rm d}^2 = \frac{\gamma-1}{qr^{\gamma}}\,\frac{qr^{\gamma}-1}{r-1}\,u_{\rm d} \equiv C_v^2\,u_{\rm d}. \tag{12}$$

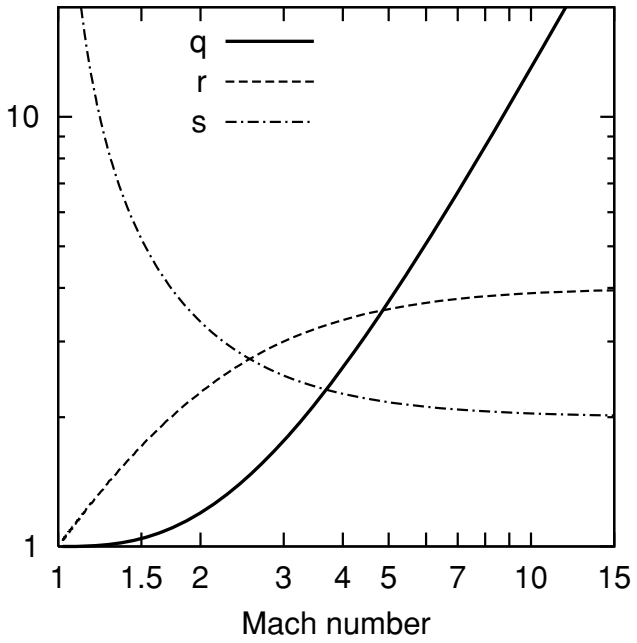


**Figure 1.** Entropy ratio, $q = S_{\rm d}/S_{\rm u}$, compression ratio, $r = \rho_{\rm d}/\rho_{\rm u}$, and spectral index, $s$, of the electron spectrum generated by DSA as a function of the Mach number.

© 2007 The Authors. Journal compilation © 2007 RAS, MNRAS **375,** 77–91

Downloaded from https://academic.oup.com/mnras/article/375/1/77/986307 by guest on 16 August 2022

### 2.2 Diffuse shock acceleration

In supernova remnants, there is evidence that electrons and protons are accelerated by DSA to energies of $\sim 10^{15}$ eV (e.g. Berezhko et al. 2003; Vink & Laming 2003). In DSA, particles are accelerated by multiple shock crossings, in a first-order Fermi process. If the shock thickness is much smaller than the diffusion scale which, in turn, has to be much smaller than the curvature of the shock front, a one-dimensional diffusion–convection equation can be solved (Axford et al. 1978; Bell 1978a,b; Blandford & Ostriker 1978). The result is that the energy spectrum of suprathermal electrons is a power-law distribution, $n_E \propto E^{-s}$. The spectral index, $s$, of the accelerated particles is only related to the compression ratio at the shock front:

$$s = \frac{r+2}{r-1}. \tag{13}$$

For strong, non-radiative shocks with Mach number $\gtrsim 10$, the compression ratio is always close to 4, hence the slope $s$ is always close to 2. This allows us to explain the spectrum of cosmic rays over a huge range of energies and may be considered as a piece of evidence for DSA. For a review of DSA, see Drury (1983), Blandford & Eichler (1987), Jones & Ellison (1991) and Malkov & O'C Drury (2001).

DSA theory suffers from the complexity of real shock fronts and the highly non-linear interaction between different processes such as cosmic rays and magnetic waves. The efficiency of accelerating electrons and protons has been inferred from the observation of supernova remnants. For instance, Dyer et al. (2001) estimated for SN 1006 that a few per cent of the shock energy is transferred to suprathermal particles. Similar to Keshet et al. (2004), we assume that a fixed fraction, $\xi_\mathrm{e}$, of thermal energy injected at the shock front goes into the acceleration of suprathermal electrons.

Moreover, we multiply the spectrum by an upper cut-off factor since electrons can only be accelerated to finite energies. Typically, the maximum energy is estimated by comparing the acceleration e-folding time and the cooling time (Keshet et al. 2003). We use here a smoothed high-energy cut-off; the reason for this particular choice will become clear in the next section. Thus, the electron spectrum generated by DSA is given by

$$n_E(E) \equiv \frac{\mathrm{d}n_\mathrm{e}}{\mathrm{d}E} = \begin{cases} n_\mathrm{e}\, C_\mathrm{spec}\, \frac{1}{m_\mathrm{e}c^2}\, \tilde{e}^{-s} \left(1 - \frac{\tilde{e}}{\tilde{e}_\mathrm{max}}\right)^{s-2} & : \quad \tilde{e} < \tilde{e}_\mathrm{max} \\ 0 & : \quad \text{elsewhere} \end{cases}, \tag{14}$$

where we have used the abbreviation $\tilde{e} = E/m_\mathrm{e}c^2$. The normalization constant can be interpreted as follows. We compute the electron number density of electrons with energies in the interval $[E, E + \Delta E]$. If we choose $E = \Delta E = m_\mathrm{e}c^2$, the number density becomes

$$n_E \Delta E = n_\mathrm{e} C_\mathrm{spec}.$$

Hence, $C_\mathrm{spec}$ gives basically the fraction of electrons at $E = m_\mathrm{e}c^2$.

We determine the fraction of suprathermal electrons by postulating that a fixed fraction, $\xi_\mathrm{e}$, of the energy injected at the shock front goes into the acceleration of electrons to suprathermal energies. After passing the shock, the downstream gas has gained a thermal energy of

$$u_\mathrm{d}\rho_\mathrm{d} - r^\gamma u_\mathrm{u}\rho_\mathrm{u} = u_\mathrm{d}\rho_\mathrm{d}\frac{q-1}{q},$$

where $r^\gamma u_\mathrm{u}\rho_\mathrm{u}$ would be the energy density after pure adiabatic compression. Hence, the spectrum can be normalized by

$$\int_{E_\mathrm{min}}^{\infty} \mathrm{d}E\; n_E(E)\; E = \xi_\mathrm{e}\, u_\mathrm{d}\rho_\mathrm{d}\frac{q-1}{q}. \tag{15}$$

A crucial parameter is the minimum energy, $E_\mathrm{min}$, above which electrons are considered to be suprathermal. It is particularly important for spectra significantly steeper than $s = 2$ since for these spectra most of the suprathermal energy is carried by electrons immediately above $E_\mathrm{min}$. Therefore, the normalization of the spectrum depends on $E_\mathrm{min}$. A hybrid simulation of a collisionless shock indicates that there is continuous transition from the thermal to the suprathermal distribution (Bennett & Ellison 1995). Simulations of electron acceleration at high Mach number shocks may rely on injection of electrons with a fixed energy. However, the typical injection energy corresponds to thermal energy in the ICM (Levinson 1994); therefore, the suprathermal spectrum is expected to be a continuous extension of the thermal spectrum. We assume here that the thermal Maxwell–Boltzmann distribution goes over continuously into the power-law spectrum of the suprathermal electrons:

$$n_E^\mathrm{Maxwell}(E_\mathrm{min}) = n_E(E_\mathrm{min}).$$

This condition leads to an implicit equation for $E_\mathrm{min}$ that has to be solved simultaneously with the normalization of the spectrum. Basically, the transition energy is tightly coupled to the temperature of the plasma:

$$E_\mathrm{min} \sim 10\, k_\mathrm{B} T,$$

if no extreme parameters are chosen.

We can write for the normalization of the electron spectrum

$$\xi_\mathrm{e}\, u_\mathrm{d}\rho_\mathrm{d}\frac{q-1}{q} = n_\mathrm{e}\, C_\mathrm{spec}\, m_\mathrm{e}c^2 \int_{\tilde{e}_\mathrm{min}}^{\infty} \mathrm{d}\tilde{e}\; \tilde{e}^{1-s} \left(1 - \frac{\tilde{e}}{\tilde{e}_\mathrm{max}}\right)^{s-2} \equiv n_\mathrm{e} C_\mathrm{spec} m_\mathrm{e}c^2 I_\mathrm{spec},$$

where

$$I_\mathrm{spec} = \int_{\tilde{e}_\mathrm{min}}^{\infty} \mathrm{d}\tilde{e}\; \tilde{e}^{1-s} \left(1 - \frac{\tilde{e}}{\tilde{e}_\mathrm{max}}\right)^{s-2}. \tag{16}$$

Downloaded from https://academic.oup.com/mnras/article/375/1/77/986307 by guest on 16 August 2022

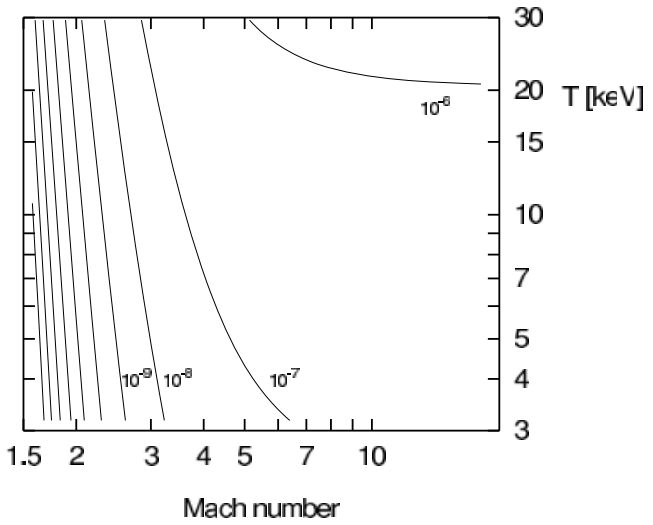


**Figure 2.** Contours of the fraction of relativistic electrons with $\gamma_{\rm L} > 300$. Contour levels are at $10^{-6}$, $10^{-7}$, $10^{-8}$, etc. The energy fraction of suprathermal electrons is $\xi_{\rm e} = 0.05$. The initial cut-off in the spectrum is at $\tilde{e} = 10^7$.

Hence, the constant becomes

$$C_{\rm spec} = \underbrace{\xi_{\rm e} \frac{u_{\rm d}}{c^2} \frac{m_{\rm p}}{m_{\rm e}}}_{C^p_{\rm spec}} \underbrace{\frac{(q-1)}{q} \frac{1}{I_{\rm spec}}}_{C^q_{\rm spec}}, \tag{17}$$

where the first factor, $C^p_{\rm spec}$, includes the plasma contributions, while the second factor, $C^q_{\rm spec}$, incorporates the dependencies from the shock strength. Since the electron spectrum is steep for Mach numbers $\lesssim$2, the fraction of relativistic electrons is low in this regime (Fig. 2). Note also that the temperature of the downstream plasma affects the relativistic electron density. For Mach numbers $\gtrsim$10, the fraction of relativistic electrons is virtually constant since the electron spectrum varies only negligibly.

In this paper, we only consider the acceleration of *electrons* in order to compute the radio emission from cosmological shocks. Clearly, there is evidence that also protons are accelerated to highly relativistic energies at shocks, probably even more efficiently than electrons (cf. Levinson 1994). Because of their larger mass, protons cause significantly less synchrotron emission than electrons. However, in inelastic collisions, relativistic protons produce electron/positron pairs which, in turn, radiate synchrotron emission. In the ICM, though, the lifetime of relativistic protons is about the Hubble time (Dennison 1980). As a result, relativistic protons gradually accumulate in the cluster potential. While the emission by secondary electrons may contaminate to some degree the emission by primary electrons, it is unlikely to account for the bulk of the radio emission from radio relics. Radio relics have a filamentary morphology and the emission is confined to regions close to the shock. This morphology is difficult to explain with suprathermal protons and is more likely caused by short-lived, primary electrons. The emission from secondary electrons and positrons produced by relativistic protons may be responsible for the cluster-wide emission observed in radio haloes. However, acceleration of protons has another consequence. Suprathermal protons can affect the pressure in the gas and thus affect the structure of the shock. An admixture of relativistic protons lowers the adiabatic exponent, $\gamma$, to below the value for a non-relativistic gas of 5/3. In the extreme case of a fully relativistic gas, $\gamma$ is 4/3. An effect of a lower $\gamma$ is that the compression ratio of the shock can be higher and, as a result, equation (13) becomes inaccurate. Moreover, the back-reaction of the relativistic particles on the shock leads to non-linear particle acceleration, which results in flatter particle spectra than the power laws obtained in the test-particle approximation. Amato & Blasi (2005) have demonstrated the effects of non-linear particle acceleration on shock structure and particle spectra. While there is some evidence for non-linear effects in supernova remnants, the details of this process remain controversial (Ellison & Cassam-Chenaï 2005). In particular, it is unclear as to what extent non-linear shock acceleration takes place in cosmological shocks. Here, we will adopt the results obtained with the linear test-particle approximation.

### 2.3 Radiative cooling of high-energy electrons

High-energy electrons in the ICM cool mainly by IC scattering with cosmic microwave background photons and by synchrotron radiation losses:

$$\frac{{\rm d}E}{{\rm d}t} = -\frac{C_{\rm cool}}{m_{\rm e}c^2} E^2, \tag{18}$$

where $E$ is the energy of an electron. The cooling constant is given by

$$C_{\rm cool} \equiv \frac{4\,\sigma_{\rm T}}{3\,m_{\rm e}\,c} (u_{\rm CMB} + u_B), \tag{19}$$

© 2007 The Authors. Journal compilation © 2007 RAS, MNRAS **375,** 77–91

Downloaded from https://academic.oup.com/mnras/article/375/1/77/986307 by guest on 16 August 2022

where $\sigma_{\rm T}$ is the Thomson cross-section, and $u_{\rm CMB}$ and $u_B$ are the energy densities of the radiation background and the magnetic field, respectively. We have neglected the effects of adiabatic cooling and heating which depend on the local flow conditions. Adiabatic cooling can, in principle, be included but for our purpose we will ignore it here. Electron number conservation leads to a partial differential equation for the energy spectrum:

$$\frac{\partial n_E}{\partial t} = C_{\rm cool}\tilde{e}^2\,\frac{\partial n_E}{\partial \tilde{e}} + 2C_{\rm cool}\tilde{e}\,n_E, \tag{20}$$

with the solution (Kardashev 1962):

$$n_E(E,t) = \begin{cases} n_{\rm e}\,C_{\rm spec}\,\frac{1}{m_{\rm e}c^2}\,\tilde{e}^{-s}\left[1-\left(\frac{1}{\tilde{e}_{\rm max}}+C_{\rm cool}t\right)\tilde{e}\right]^{s-2} & : \quad \tilde{e}\,C_{\rm cool}\,t < 1-\tilde{e}/\tilde{e}_{\rm max} \\ 0 & : \quad \text{elsewhere} \end{cases}. \tag{21}$$

We have chosen the cut-off factor in equation (14) consistently with this solution, hence the initial spectrum is already a solution to equation (20).

The energy densities of the cosmic radiation background with temperature $T_{\rm CMB} = T_{\rm CMB,0}(z+1)$ and of the downstream magnetic field, $B_{\rm d}$, are

$$u_{\rm CMB} = a_{\rm rad}\,T_{\rm CMB,0}^4\,(z+1)^4 \equiv \frac{B_{\rm CMB}^2}{8\pi} \tag{22}$$

and

$$u_B = \frac{B_{\rm d}^2}{8\pi}, \tag{23}$$

respectively, where $z$ is the redshift and $a_{\rm rad}$ is the radiation constant. For convenience, we have introduced a magnetic field equivalent for the background radiation, $B_{\rm CMB}$. For $z = 0$, $B_{\rm CMB}$ is about 3.24 μG. Since we are primarily interested in radio emission which is produced by relativistic electrons, it is convenient to express the related equations in terms of the Lorentz factors, $\gamma_{\rm L}$, of the electrons. Only electrons with $\gamma_{\rm L} \gg 1$ contribute significantly to the radio emission and we can approximate the Lorentz factor

$$\gamma_{\rm L} = \frac{E}{m_{\rm e}c^2} + 1 \approx \frac{E}{m_{\rm e}c^2} = \tilde{e} \qquad \text{for} \qquad E \gg m_{\rm e}c^2. \tag{24}$$

For any observing frequency, there is a minimum Lorentz factor below which the radio emission is negligible. On the other hand, equation (21) shows that the electron spectrum has a time-dependent, maximum energy. For any Lorentz factor, we can determine the time when the maximum energy in the spectrum equals the given $\gamma_{\rm L}$, which is given by

$$t_{\rm cool}(\gamma_{\rm L}) = \frac{1}{C_{\rm cool}\,E(\gamma_{\rm L})} = 2.32\times10^{12}\,\gamma_{\rm L}^{-1}\,(z+1)^{-4}\,{\rm yr},$$

where the right-hand expression is computed for pure IC cooling (we have assumed here that $\tilde{e}/\tilde{e}_{\rm max} \ll 1$). After a time $t_{\rm cool}(\gamma_{\rm L})$, there are no electrons with Lorentz factor above $\gamma_{\rm L}$.

### 2.4 The synchrotron emission

The synchrotron power of a single electron, $P_{\rm e}$, that moves with a Lorentz factor $\gamma_{\rm L}$ in a magnetic field $B$ is (for an introduction see Rybicki & Lightman 1979):

$$\frac{{\rm d}P_{\rm e}(\gamma_{\rm L},\,\nu_{\rm obs})}{{\rm d}\nu} = \frac{\sqrt{3}\,e^3 B\,\sin\alpha}{m_{\rm e}c^2}\,F\left(\frac{\nu_{\rm obs}}{\nu_{\rm c}}\right) \equiv C_{\rm sync}\,F\left(\frac{\nu_{\rm obs}}{\nu_{\rm c}}\right), \tag{25}$$

where $e$ is the electron charge, $\alpha$ the angle enclosed between the direction of the motion and the magnetic field, and $\nu_{\rm c}$ is the characteristic frequency given by

$$\nu_{\rm c} = \frac{3\gamma_{\rm L}^2 eB\,\sin\alpha}{4\pi\,m_{\rm e}c}.$$

In the following, we assume that the directions of the electron motion and the magnetic field are uncorrelated, therefore we take the average value $\langle\sin\alpha\rangle = \pi/4$, where the average is over solid angle. The function $F(x)$ has to be integrated numerically:

$$F(x) = x\int_x^\infty {\rm d}\xi\;K_{5/3}(\xi),$$

where $K$ is the modified Bessel function. The emission per volume is given by the convolution

$$\frac{{\rm d}^2P(\nu_{\rm obs})}{{\rm d}V\,{\rm d}\nu} = \int_0^\infty {\rm d}E\,n_E P_{\rm e} = C_{\rm sync}\int_0^\infty {\rm d}\gamma_{\rm L}\,m_{\rm e}c^2\,n_E(\gamma_{\rm L},t)\,F(\gamma_{\rm L},\,\nu_{\rm obs}).$$

We introduce a new variable

$$\tau \equiv \sqrt{\frac{3\,eB}{\nu_{\rm obs}\,16\,m_{\rm e}c}}\;\gamma_{\rm L} \equiv C_\tau\,\gamma_{\rm L} = 4.85\times10^{-5}\left(\frac{B}{\mu{\rm G}}\right)^{1/2}\left(\frac{1.4\,{\rm GHz}}{\nu_{\rm obs}}\right)^{1/2}\gamma_{\rm L}. \tag{26}$$

Substituting $\gamma_{\rm L}$ by $\tau$, the integration becomes

$$\frac{{\rm d}^2P(\nu_{\rm obs})}{{\rm d}V\,{\rm d}\nu} = \frac{C_{\rm sync}\,m_{\rm e}c^2}{C_\tau}\int_0^\infty {\rm d}\tau\;n_E(\tau,t)\,F\left(\frac{1}{\tau^2}\right). \tag{27}$$

Downloaded from https://academic.oup.com/mnras/article/375/1/77/986307 by guest on 16 August 2022

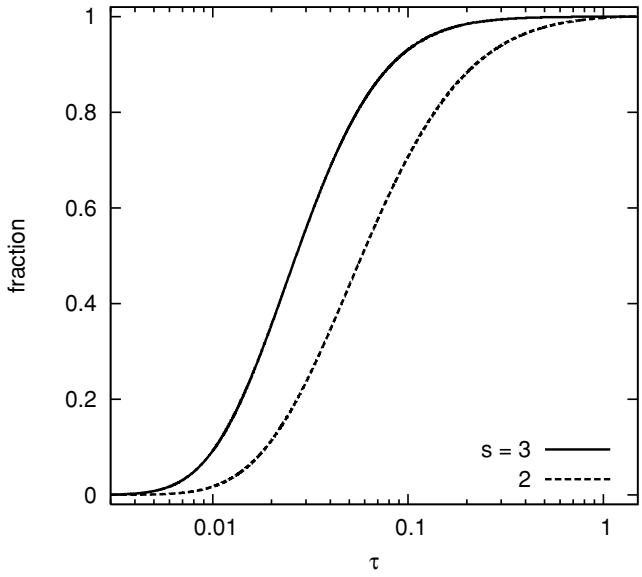


**Figure 3.** Cumulative synchrotron emission. Computed according to equation (27) assuming a power law for the electron energy spectrum, $n_E(\tau) \propto \tau^{-s}$.

Assuming a power-law spectrum for $n_E$, we compute the cumulative emission (Fig. 3). The bulk of the emission comes from $\tau_{\rm half} \sim 0.03$. This implies that electrons with Lorentz factors of about

$$\gamma_{\rm L,half} = 6.2 \times 10^2 \left(\frac{\mu{\rm G}}{B}\right)^{1/2} \left(\frac{\nu_{\rm obs}}{1.4\,{\rm GHz}}\right)^{1/2} \tag{28}$$

contribute most to the synchrotron emission. Note that at $\gamma_{\rm L} \sim 3 \times 10^2$ and below, Coulomb losses constitute the most important cooling mechanism for suprathermal electrons, see e.g. Sarazin (1999). Hence, at very low observing frequencies in regions with a rather strong magnetic field, Coulomb cooling becomes important. For instance, LOFAR may observe at 30 MHz a radio halo region where the magnetic field is of the order of 3 μG. Equation (28) indicates that the bulk of the radio emission would come from electrons with Lorentz factor $\gamma_{\rm L} \sim 50$. For such low Lorentz factors, Coulomb cooling is important; hence, our analysis may overestimate the synchrotron emission at very low observing frequencies.

### 2.5 Total emission behind the shock front

In Section 2.2, we worked out the relativistic spectrum of electrons accelerated at the shock front, in Section 2.3 we worked out the evolution of the spectrum subject to cooling, and in Section 2.4 we computed the synchrotron emissivity for a homogeneous electron population. Now we combine these results, to compute the total emission behind the shock front. We adopt the following scenario. DSA generates a population of suprathermal electrons. In energy space, these electrons are distributed initially according to a power law. While they advect with the downstream plasma, the relativistic electrons cool by synchrotron and IC losses. With increasing distance to the shock front, the maximum electron energy decreases and the radio emission diminishes. The total emission is obtained by summing up all contributions from the plasma from the shock front to the distance where the electron spectrum is too cool to allow any further radio emission.

To compute the spatial distribution of the emission, we have to model the downstream region of the shock front. Instabilities of waves propagating at the shock surface presumably originate turbulence in the downstream plasma immediately behind the shock surface. Whether this turbulence can also be found at larger distances from the shock surface depends strongly on the viscosity of the ICM, which is still rather uncertain (see e.g. Fabian et al. 2005). If the viscosity is indeed close to the Spitzer value of a hot plasma, as suggested by the H$\alpha$ filaments surrounding NGC 1275, the formation of turbulence would be significantly hampered. Hence, we assume the flow in the downstream region to be steady and laminar.

Diffusion can alter the spatial distribution of suprathermal electrons. In the absence of magnetic fields, the diffusion length is dominated by Coulomb collisions. The presence of even very weak magnetic fields suppresses diffusion in various ways. In directions perpendicular to magnetic field lines, electrons propagate roughly with the Bohm diffusion rate. The resulting distance covered within the cooling time of even very energetic particles is negligible for our purposes. Parallel to the magnetic field lines, the electrons propagate with the drift velocity, provided the gyroradius is significantly smaller than the coherence length of the magnetic field. The gyroradius of relativistic electrons is given by

$$r_{\rm g} = \gamma_{\rm L} \frac{m_{\rm e}c^2}{eB} \approx 6 \times 10^{-8}\,{\rm kpc} \left(\frac{\gamma_{\rm L}}{10^4}\right) \left(\frac{B}{1\,\mu{\rm G}}\right)^{-1}.$$

© 2007 The Authors. Journal compilation © 2007 RAS, MNRAS **375,** 77–91

Downloaded from https://academic.oup.com/mnras/article/375/1/77/986307 by guest on 16 August 2022

Hence, the gyroradius of suprathermal electrons in the ICM is of the order of $10^{12}$–$10^{14}$ cm. The correlation length of magnetic fields generated at the shock surface is expected to be of the order of $10^{10}$ cm (Medvedev, Silva & Kamionkowski 2006), but it is also expected to increase rapidly (Medvedev et al. 2005). As a result, electrons drift virtually freely along the field lines. Thus, diffusion along field lines is the most efficient transport; any tangling of field lines inside the gyroradius reduces the diffusion (Colafrancesco & Blasi 1998). The electron drift is hampered by pitch angle scattering with plasma waves, in particular with Alfvén waves (Wentzel 1974). These waves are generated by fast electrons and protons that move with super-Alfvén speed. Thus, collective effects in the plasma suppress the drift parallel to the field lines. Even if the precise treatment of electron diffusion is impossible since the actual state of the downstream plasma is not very well known, the collective effects seem to restrict the diffusion of suprathermal electrons to much smaller scales than those that we discuss in the context of radio relics (Section 3). This allows us to assume that relativistic electrons purely advect with the plasma. Similar conclusions have been drawn in related studies that show, for example, that radio haloes cannot be explained by the diffusion of electrons from a central radio galaxy (Jaffe 1977; Dennison 1980; Fujita & Sarazin 2001).

We now compute the total emission from the downstream region. The total emission per shock surface area $A$ is given by the integral over the whole downstream region, the width of which is here parameterized by $y$:

$$\frac{\mathrm{d}^2 P(\nu_{\rm obs})}{\mathrm{d}A\,\mathrm{d}\nu} = \int_0^\infty \mathrm{d}y \int_{E_{\rm min}}^\infty \mathrm{d}E\; n_E(E,t)\, P(\gamma_{\rm L}, \omega_{\rm obs}). \tag{29}$$

In any given volume element, the electron spectrum depends on the time passed since the acceleration at the shock front due to cooling. If we assume that the suprathermal electrons advect with the plasma at constant speed, the distance to the shock front and the time passed since acceleration are related by $y = v_{\rm d} t$. Hence, we can write

$$C_{\rm cool}\,\tilde{e}\,t = C_{\rm cool}\,\gamma_{\rm L}\,\frac{y}{v_{\rm d}} = \frac{C_{\rm cool}}{C_\tau v_{\rm d}}\,\tau\, y.$$

Using the following substitution:

$$\eta = \frac{C_{\rm cool}}{C_\tau v_{\rm d}}\, y, \tag{30}$$

the integral equation (29) becomes

$$\frac{\mathrm{d}^2 P(\nu_{\rm obs})}{\mathrm{d}A\,\mathrm{d}\nu} = C_{\rm all} \int_0^\infty \mathrm{d}\eta \int_{\tau_{\rm min}}^\infty \mathrm{d}\tau\; \tau^{-s}\,(1-\tau\eta)^{s-2}\, F\left(\frac{1}{\tau^2}\right) \equiv C_{\rm all} I_\Psi(s). \tag{31}$$

The lower limit, $\tau_{\rm min}$, is, in principle, defined by the energy where the energy spectrum goes from thermal to suprathermal. However, as discussed above, the bulk of the radiation comes from the region with $\tau \sim 0.03$, which is by orders of magnitude above the value of $\tau_{\rm min}$. Thus, we are free to use 0 as lower integration limit. The rapid decrease in $F(1/\tau^2 \to \infty)$ ensures that the integrand is well behaved. As a result, the integral depends only on the spectral index of the electron spectrum, $s$.

Substituting the normalization of the electron spectrum, equation (21), the emission of a homogenous volume equation (27), and equation (30) to the total emission equation (31), we find

$$C_{\rm all} = m_{\rm e}c^2 \left(\frac{C_{\rm sync}}{C_\tau}\right) n_{\rm e} C_{\rm spec} \frac{1}{m_e c^2} C_\tau^s \left(\frac{C_\tau v_{\rm d}}{C_{\rm cool}}\right) = n_{\rm e}\, C_{\rm spec}\, C_{\rm sync}\, C_\tau^s\, \frac{C_v \sqrt{u_{\rm d}}}{C_{\rm cool}},$$

where we have also used $v_{\rm d} = C_v \sqrt{u_{\rm d}}$ (equation 12). Now, it is useful to combine all factors that depend on the strength of the shock in equation (31) in

$$\begin{aligned}\Psi(\mathcal{M}) &= C_\Psi\, C_v(\mathcal{M})\; [C_\tau(1\;\mu\mathrm{G}, 1.4\;\mathrm{GHz})]^s\; C_{\rm spec}^q\; I_\Psi \\ &= \frac{(4.85\times10^{-4})^s}{2.07\times10^{-9}} \frac{(q-1)}{q} \sqrt{\frac{(\gamma-1)}{q r^\gamma}\frac{q r^\gamma - 1}{(r-1)}}\; \frac{I_\Psi}{I_{\rm spec}},\end{aligned}$$

where the normalization constant $C_\Psi$ has been determined by the condition $\Psi(\mathcal{M} \to \infty) = 1$. We note that there is also a weak dependency from the downstream plasma temperature via the integral $I_{\rm spec}$. However, for weak shocks, $\mathcal{M} \lesssim 3$, the expression $\Psi$ decreases rapidly (Fig. 4), while it is virtually constant with $\Psi \sim 1$ for strong shocks. This implies that rather strong shocks with Mach numbers $\mathcal{M} \gtrsim 3$ are necessary to produce any observable radio emission.

After subsuming the terms governed by the strength of the shock under $\Psi(\mathcal{M})$, we rewrite the total emission equation (31) in the form

$$\begin{aligned}\frac{\mathrm{d}P(\nu_{\rm obs})}{\mathrm{d}\nu} &= A\, n_{\rm e}\, C_{\rm spec}^p\, C_{\rm sync} \left(\frac{B}{\mu\mathrm{G}}\right)^{s/2} \left(\frac{1.4\;\mathrm{GHz}}{\nu_{\rm obs}}\right)^{s/2} \frac{\sqrt{u_{\rm d}}}{C_{\rm cool}} \frac{1}{C_\Psi}\, \Psi(\mathcal{M}) \\ &= 6.4\times10^{34}\,\mathrm{erg\,s^{-1}\,Hz^{-1}}\, \frac{A}{\mathrm{Mpc}^2}\, \frac{n_{\rm e}}{10^{-4}\,\mathrm{cm}^{-3}}\, \frac{\xi_{\rm e}}{0.05} \left(\frac{\nu_{\rm obs}}{1.4\;\mathrm{GHz}}\right)^{-s/2} \\ &\quad \times \left(\frac{T_{\rm d}}{7\;\mathrm{keV}}\right)^{3/2} \frac{(B/\mu\mathrm{G})^{1+(s/2)}}{(B_{\rm CMB}/\mu\mathrm{G})^2 + (B/\mu\mathrm{G})^2}\, \Psi(\mathcal{M}).\end{aligned} \tag{32}$$

Note that the emission follows a power law $\propto \nu^{-s/2}$, and thus for $s = 2$ it goes as $\propto \nu^{-1}$. Since $\Psi(\mathcal{M}) \leqslant 1$ and $B^{1+s/2}/(B_{\rm CMB}^2 + B^2) \leqslant 1$ for $s = 2$, the factor in front, $6.4\times10^{34}\,\mathrm{erg\,s^{-1}\,Hz^{-1}\,Mpc^{-2}}$, poses an upper limit for the synchrotron emission with respect to the Mach number of the shock and the strength of the magnetic field.

Downloaded from https://academic.oup.com/mnras/article/375/1/77/986307 by guest on 16 August 2022

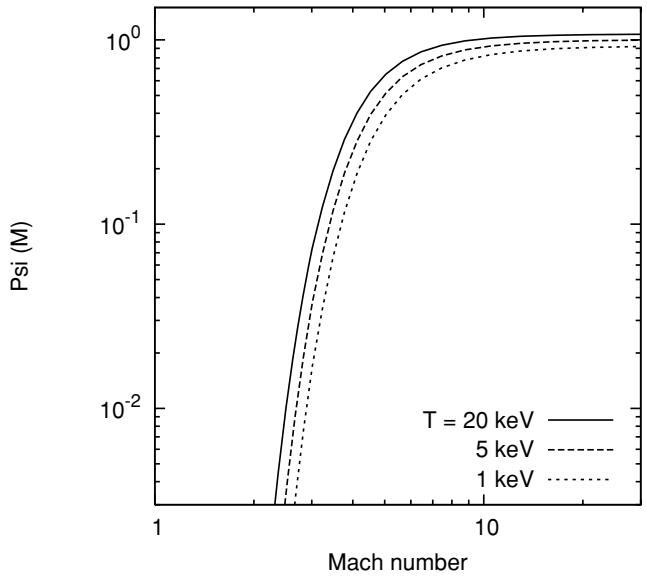


**Figure 4.** $\Psi$ as a function of the Mach number. Also the downstream temperature has a small impact.

If a radio relic is seen edge-on, its extension perpendicular to the shock front can be determined. From our model, we can compute at which distance, $y_c$, the synchrotron emission in the downstream region decreases to a fraction (which we somewhat arbitrarily set to 30 per cent) of its value immediately behind the shock front. We use such a rather high fraction since up to 10 per cent of the emission comes from electrons with $\tau \lesssim 0.01$ (Fig. 3). With the help of equation (26), we can derive the corresponding Lorentz factor. For instance, in a region with a magnetic field of 4 μG and with an observing frequency of 1.4 GHz, 10 per cent of the synchrotron emission is originated by electrons with $\gamma_L \lesssim 100$. The spectral electron density in this energy range, however, would be significantly diminished by Coulomb cooling, which is not included in our analysis. Thus, the distance where the emission diminishes to 30 per cent of the initial value seems to be a realistic estimate for the extension of the observable region.

To obtain the width of the emission region, we derive first the dimensionless distance $\eta_c$, where $\eta$ has been introduced in equation (30). The emission depends on the distance to the shock front, that is, $\eta$, via the integral $\int \ldots d\tau$ in equation (31). We compute at which $\eta_c$ this integral drops to 30 per cent of its value for $\eta = 0$. Since the integration depends on the slope of the electron spectrum, $s$, so does $\eta_c$. We find a linear dependence, namely $\eta_c(s) = 4.8 \times s - 1.5$. Using the definition of $\eta$, we derive the effective width of the emission region as

$$y_c = \frac{C_\tau\, v_d}{C_{cool}}\,\eta_c = 120\,\mathrm{kpc}\;\frac{(B/\mu\mathrm{G})^{1/2}}{(B_{CMB}/\mu\mathrm{G})^2 + (B/\mu\mathrm{G})^2}\left(\frac{\nu_{obs}}{1.4\,\mathrm{GHz}}\right)^{s/2}\frac{v_d}{100\,\mathrm{km\,s^{-1}}}\,\eta_c. \tag{33}$$

This equation shows the dependence of the width of the relic, $y_c$, on the magnetic field. In the regime of small magnetic field strengths, $B \ll B_{CMB} = 3.2$ μG (for $z = 0$), $y_c$ is proportional to $B^{1/2}$. Higher magnetic fields produce thicker relics because a higher magnetic field lowers the relevant Lorentz factor for synchrotron emission. In contrast, in a regime with strong magnetic field, $B \gg B_{CMB}$, the $y_c$ shrinks with increasing B-field according to $y_c \propto B^{-3/2}$ due to the synchrotron cooling itself. The width, $y_c$, is maximal for $B \sim 2$ μG (Fig. 5).

Also the strength of the shock affects the size of the synchrotron emitting area. Rather weak shocks, $\mathcal{M} \lesssim 3$, are more extended, since the spectrum is steeper. For a spectral index of $s = 3$, electrons with smaller $\tau$ are mainly responsible for the emission than for $s = 2$ (Fig. 3). Hence, it takes longer to diminish the density of the relevant electron population. For small $\tau$, that is, weak shocks and strong magnetic fields, the electron population is strongly reduced by Coulomb cooling, which is not included in our model. For those shocks, the extension of the emission area is smaller than that which is predicted here.

We can also derive the time after which the emission of the downstream plasma has dropped to 30 per cent of its initial value from equation (33):

$$t_c = \frac{y_c}{v_d} = \frac{C_\tau v_d}{C_{cool}}.$$

It has a maximum at $B \sim 2$ μG, which amounts to ∼1 Gyr for $\mathcal{M} = 4$.

The code for computing the synchrotron emission and the width of the emission region will be provided upon request.

## 3 CLUSTER RADIO RELIC EXAMPLES

### 3.1 Abell 3667

A textbook example of a merging cluster with strong shocks travelling into the cluster periphery is Abell 3667. This cluster is unique since it shows prominent radio emission (Röttgering et al. 1997) which is presumably caused by an outgoing shock wave. In X-rays, there is a double

© 2007 The Authors. Journal compilation © 2007 RAS, MNRAS **375,** 77–91

Downloaded from https://academic.oup.com/mnras/article/375/1/77/986307 by guest on 16 August 2022

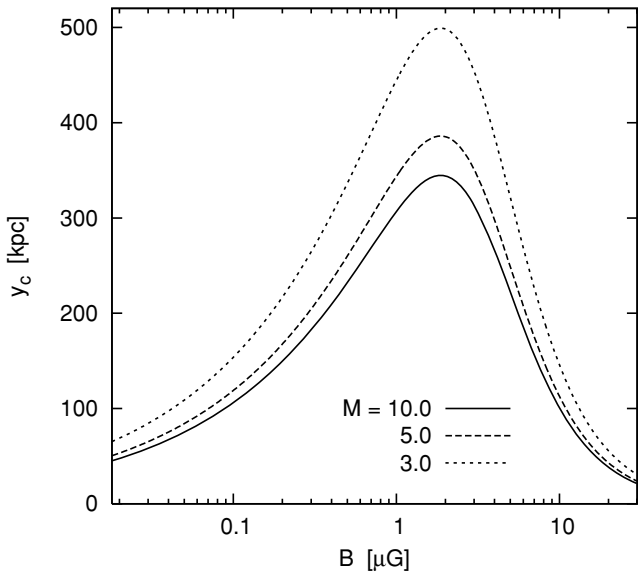


**Figure 5.** The distance at which the radio emission decreases to 30 per cent of the value at the shock front.

peak in the cluster centre (Shibata et al. 1999) and a cold front indicating a fast moving substructure (Markevitch et al. 2002). Both, indicates that the cluster suffered a merger recently. Even if the X-ray flux from the cluster periphery is not sufficient to identify a shock front at the position of relics, Roettiger et al. (1999) showed that X-ray morphology and position of the relics is consistent with a merger of a 20 per cent substructure 1 Gyr ago. The spectral index of the north-west relic varies clearly: it steepens from $\alpha \sim 0.6$ at the outer rim to 1.5 at its faint rim towards the cluster centre. This suggests that the relic is basically seen edge-on: the outer rim is populated by recently accelerated electrons, while towards the centre, the electrons population has aged.

A similar steepening of the electron spectrum is expected in our model. As the plasma moves downstream and the electrons age, the radio spectrum steepens. However, the overall spectrum is a power law (equation 32), even if locally the spectrum may steepen towards higher frequencies. Note that the power law is only obtained if all contributions to the total emission are present: from the newly accelerated electron population at the shock front up to the old electrons that are too cold to emit significant synchrotron radiation. In order to apply our model to this relic, the downstream region should be homogeneous, that is, it should not show adiabatic contraction in this region, etc. The north-west relic in Abell 3667 is quite close to such an ideal scenario. Röttgering et al. (1997) found an overall index of $\alpha = 1.1$. They argued that there is no spectral steepening, what may indicate that we see plasma from the injection to the point where the emission has faded. Using equation (32), we conclude that the initial slope in the electron spectrum is $s = 2.2$, which is consistent with $\alpha \sim 0.6$, close to the shock surface. [For a homogenous distribution of suprathermal electron with power-law spectral slope, $s$, the radio emission has the spectral index $\alpha = (s - 1)/2$.] By combining equations (8), (11) and (13), we can also infer the Mach number of the shock. We find that the Mach number of the shock related to the north-west relic in Abell 3667 is $\mathcal{M} = 4.7$.

We can use our expression for the total emission to estimate the field strength in the downstream region. Röttgering et al. (1997) derived the temperature and electron density in the relic region to be $10^8$ K and $10^{-4}$ cm$^{-3}$, respectively. Sarazin (1999) argued that about 1 per cent of the thermal energy in the ICM is found in relativistic electrons, with $\gamma_L > 300$. Since our definition of $\xi_e$ includes also suprathermal electrons with $\gamma_L < 300$, we choose a somewhat higher value of $\xi_e = 0.05$. In order to compute the total emission, we also need the area of the shock surface. From Röttgering et al. (1997, fig. 4), we estimate that the bulk of radio emission is extended over ∼2.0 Mpc. Using these ICM parameters, we derive the radio emission as a function of the shock strength and the downstream magnetic field (Fig. 6). The observed total emission is $P_{1.4} = 4.1 \times 10^{32}$ erg s$^{-1}$ Hz$^{-1}$. We have derived the Mach number of the shock by the spectral index of the radio emission. By comparing the observed radio power to the computed emission (Fig. 6), we conclude that the strength of the magnetic field in the relic region is $B \sim 0.2$ μG.

Since this relic is basically seen edge-on, its extension perpendicular to the shock front, that is, radial with respect to the cluster centre, can be used to infer the magnetic field strength. In Section 2.5, we have introduced a width $y_c$, which is the shortest distance between the shock front and the downstream position where the radio emission has decreased to 30 per cent of its value at the shock front. The temperature of the downstream plasma and the Mach number of the shock determine the dimensionless quantity $\eta$ and the downstream velocity, $v_d$. For the parameters of Abell 3667, we obtain 9.0 and 720 km s$^{-1}$, respectively. With a magnetic field of 0.2 μG, we derive from equation (33) that the width $y_c$ amounts to 0.3 Mpc, which is consistent with the observed extension of the relic.

If the gas in the downstream region is substantially compressed, the relativistic electrons are re-energized by adiabatic compression. For a polytropic gas with $\gamma = 5/3$, the gas density in the periphery of cluster scales with $\rho_{gas} \propto [\ln(1 + r/r_s)/(r/r_s)]^{3/2}$, where $r$ is the distance from the cluster centre and $r_s$ is the scaling radius of the cluster (Ascasibar et al. 2006). Most relics are situated on the periphery of galaxy clusters. The radio relics in Abell 3667, for example, are located at distances of ∼2.6 Mpc on either side from the cluster centre. Given that

Downloaded from https://academic.oup.com/mnras/article/375/1/77/986307 by guest on 16 August 2022

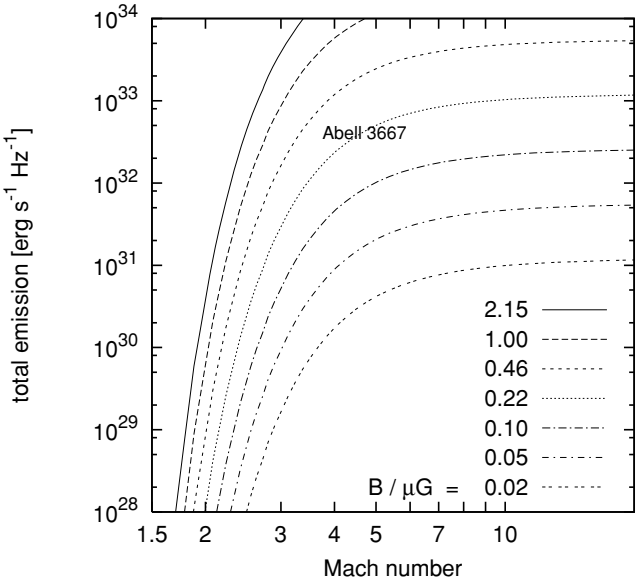


**Figure 6.** Radio power as a function of Mach number for different magnetic field strengths. We have marked the position of the radio power and the derived Mach number for Abell 3667.

the relics have a width of around 300 kpc and assuming that the downstream gas density follows the density profile of the cluster, the density increase along the relic is no more than ∼15 per cent. Such a small compression has a moderate effect on the average electron energy (cf. Enßlin & Gopal-Krishna 2001). Flux conservation leads to $B \propto \rho^{2/3}$, hence the magnetic field can be enhanced maximally a few ten per cent. Hence, we neglect the effects of adiabatic compression in the following discussion.

### 3.2 Abell 115

Another example of a very extended radio relic has been found in Abell 155. Its size tangential to the cluster X-ray emission is more than 2 Mpc. In contrast, it is very thin in radial direction, a few hundred kpc at most. Compared to Abell 3667, it has a much lower radial/tangential extension ratio. Obviously, such a thin radio structure can only be achieved when the line of sight is tangential to the shock surface. Another prerequisite is that the radio emission fades quickly while the plasma moves downstream. Considering the discussion above, this implies a low magnetic field strength in the downstream plasma.

Similar to the procedure used for the north-west relic in Abell 3667, we can infer the magnetic field strength in the emission region. We adopt the values given by Shibata et al. (1999) for Abell 115. The cluster temperature in the periphery is about 5 keV, and the electron density is of the order of $10^{-4}$ cm$^{-3}$. The total radio emission in A115 is $P_{1.4} = 1.9 \times 10^{32}$ erg s$^{-1}$ Hz$^{-1}$ with slope $\alpha = 1.1$. (Govoni et al. 2001b – note that there was a typographical error in that paper; the flux of A115 is actually an order of magnitude higher than given; Govoni, private communication). Other parameters are used as given above, e.g., the energy fraction in suprathermal electrons $\xi_e$. Since the spectral slope is the same as in Abell 3667, the Mach number of the shock is again $\mathcal{M} = 4.7$. The lower temperature in the downstream region also lowers the radio emission. We find that a similar magnetic field strength as in A3667, namely $B \sim 0.1$ μG, reproduces the observed emission well.

In the direction perpendicular to the shock front, the emission has dropped to 30 per cent of its initial value at a distance of 0.15 Mpc from the shock front. This value is also consistent with the observations.

### 3.3 Abell 2256

Abell 2256 shows a radio halo and relic (Clarke & Ensslin 2006). The relic is seen close to face-on, hence the spectral steepening is only mild. The average slope is $\alpha = -1.2$, which indicates a shock with Mach number $\mathcal{M} = 3.3$. From Rephaeli & Gruber (2003), we adopt a cluster temperature of 7.8 keV. The observed extension of the relic is about 1 Mpc; hence, we assume a shock surface area of 1 Mpc$^2$. The power $P_{1.4} = 3.6 \times 10^{31}$ erg s$^{-1}$ Hz$^{-1}$ is reproduced, provided the magnetic field has a strength of $B \sim 0.3$ μG.

This value for the magnetic field is almost a magnitude lower than that in the central halo region (see Clarke & Ensslin 2006) and indicates that the magnetic field decreases with increasing radius from the centre.

If the radio relic is being produced by a giant shock wave, what has produced the radio halo in Abell 2256? Can the two phenomena be linked? With the magnetic field in the plasma also the relevant Lorentz factor for the radio emission changes. If the magnetic field in the halo region is about a few μG as indicated by Clarke & Ensslin (2006), the Lorentz factor of those electrons that produce the radio emission is $\gamma_{\rm L,half} \sim 300$. In contrast, in the relic region the lower magnetic field implies that the Lorentz factor of the radio-emitting electrons is $\gamma_{\rm L,half} \sim 1000$. At the field strengths in both relic and halo, we can assume that the cooling of the electron spectrum is mainly caused by IC

© 2007 The Authors. Journal compilation © 2007 RAS, MNRAS **375,** 77–91

Downloaded from https://academic.oup.com/mnras/article/375/1/77/986307 by guest on 16 August 2022

**Table 1.** Observed and derived parameters for our three model relics. For all computations, we have assumed an electron density of $n_e = 10^{-4}$ cm$^{-3}$. LLS indicates the longest linear size of a relic. To determine the radio power of the relics, we use $H_0 = 50$ km s$^{-1}$ Mpc$^{-1}$ in order to be consistent with computations in the literature.

| | $z$ | $T$ (keV) | LLS (Mpc) | $P_{1.4}$ ($10^{31}$ erg s$^{-1}$ Hz$^{-1}$) | $\alpha$ | $M$ | $B$ ($\mu$G) | $y_c$ (Mpc) | $\xi_B$ ($10^{-3}$) |
|---|---|---|---|---|---|---|---|---|---|
| Abell 115 | 0.1971 | 5 | 2.5 | 1.9 | 1.1 | 4.7 | 0.1 | 0.1 | 0.2 |
| Abell 2256 | 0.0594 | 7.8 | 1.1 | 3.6 | 1.2 | 3.3 | 0.3 | 0.4 | 1.1 |
| Abell 3667 | 0.055 | 8 | 2.0 | 41.0 | 1.1 | 4.7 | 0.2 | 0.3 | 0.5 |

cooling. Since the cooling time is inversely proportional to $\gamma_L$, the cluster core would emit synchrotron radiation three times longer. Hence, it is conceivable that the halo and relic are caused by the same shock front.

## 4 RADIO EMISSION VERSUS CLUSTER TEMPERATURE

The example clusters discussed above indicate that shocks which produce presently observable radio emission have Mach numbers of about $\mathcal{M} \sim 3$–5. It is interesting to note that significantly stronger shocks show only moderately more radio emission if all other downstream parameters are the same as shown in Fig. 4. This is due to the fact that strong shocks reach an asymptotic slope for the electron spectrum. Much weaker shocks would have virtually no radio emission. Gabici & Blasi (2003) found that it is quite unlikely to achieve shock strength of $\mathcal{M} \gtrsim 4$ in a cluster merger. The combination of the paucity of shocks with $\mathcal{M} \gtrsim 4$ and the strong suppression of radio emission in weaker shocks may explain to some extent why only so few radio relics have been found.

If we consider the magnetic field dependency in equation (32), one striking feature is that for strong field strengths, $B \gg B_{\rm CMB}$, the emission is constant. Hence, even an arbitrarily strong shock with an arbitrarily strong magnetic field would not exceed an emission of $\sim 6 \times 10^{34}$ erg s$^{-1}$ Hz$^{-1}$, with standard parameters for temperature and density. Thus, there is a distinct upper limit for the radio emission. Intriguingly, our few examples support the assumption that the magnetic field in the ICM is correlated with its temperature. We found that Abell 3667 and 2256 which have temperatures of about 8 keV lead to magnetic field strengths of 0.2–0.3 $\mu$G. In contrast, A115 with a temperature of 5 keV shows a field strength of 0.1 $\mu$G in the relic region. However, we restrict ourselves here to the custom assumption that a fraction, $\xi_B$, of the energy dissipated at the shock front is converted into magnetic fields:

$$\frac{B^2}{8\pi} = \xi_B \, m_p n_e u. \tag{34}$$

On average, the magnetic field energy fraction is $\langle \xi_B \rangle = 6 \times 10^{-4}$ for our example clusters (Table 1). Thus, only a very small fraction of the dissipated energy has to be converted. For Abell 115 and 2256, the values of $\xi_B$ may be underestimated to some extent, since we have assumed that, at the location of the relics, the plasma has the average cluster temperature. Only for Abell 3667, a temperature estimate for the relic region is available. However, we use equation (37) to compute the radio power as a function of the cluster temperature (Fig. 7, solid

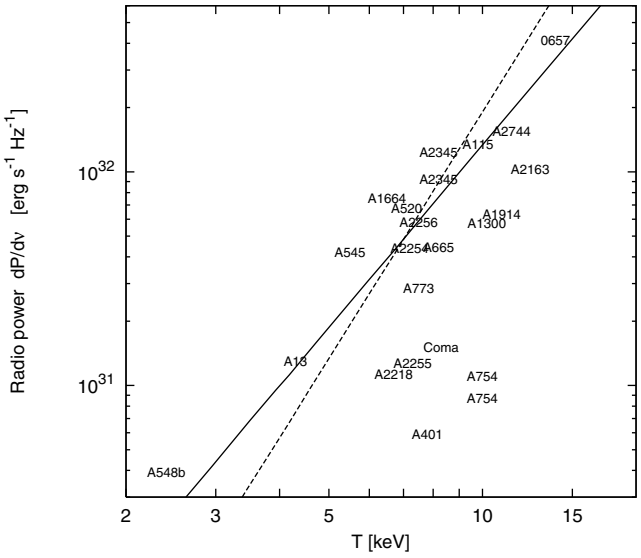


**Figure 7.** Radio power for an observing frequency of 1.4 GHz versus cluster temperature. The solid line indicates the radio power for a shock front with an area of 1 Mpc$^2$, while the dashed line is computed for a temperature-dependent area, $A \propto T$ (Fig. 8). Radio and X-ray data for the clusters are taken from Giovannini et al. (1999), Govoni et al. (2001b) and Govoni et al. (2004).

Downloaded from https://academic.oup.com/mnras/article/375/1/77/986307 by guest on 16 August 2022

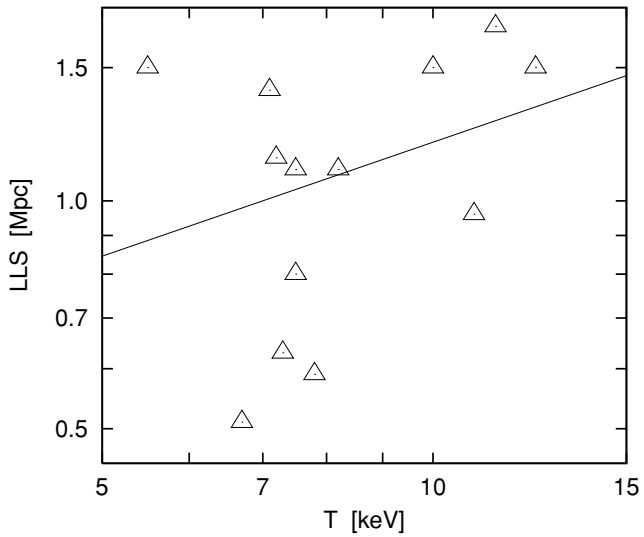


**Figure 8.** Longest linear size (LLS) versus cluster temperature for radio haloes shown in Fig. 7. The solid line indicates LLS $= 1$ Mpc $(T/7\ \mathrm{keV})^{1/2}\ T$.

line). Here, we have assumed that the typical strength of a strong shock in the ICM is $\mathcal{M} = 4$ and that the length-scale of the shock fronts is 1 Mpc.

Our estimate for the radio emission is close to the emission observed for radio haloes. This may indicate that a significant part of the radio halo emission may be the result of an earlier merger shock. The observed radio power–temperature relation seems to be steeper than our result. This may be attributed to scaling relations that we have ignored in our analysis. It seems plausible that the linear size of radio haloes depends on the cluster temperature (Fig. 8). On average, one may expect that the extension of haloes is a fraction of the virial radius, $r_{\rm vir}$ which scales with the cluster temperature by $r_{\rm vir} \propto M^{1/3} \propto T^{1/2}$ (for cluster scaling relations see e.g. Eke, Navarro & Frenk 1998). Including the linear size–temperature relation into our estimate for the radio power, we obtain a somewhat steeper dependency (Fig. 7). The slope of the radio power is now $\mathrm{d}P/\mathrm{d}\nu \propto T^{(12+s)/4}$ (equation 32), where we have used $B^2 \propto T$ and $A \propto T$. Hence, the strong temperature dependence is caused by the combination of several facts: With increasing cluster temperature, the electron density in the relevant Lorentz factor regime increases, the magnetic field scales with the temperature, and the average linear size of the emission increases with cluster temperature, that is, its mass.

## 5 COSMIC ACCRETION SHOCKS

Numerical simulations suggest that structure formation shocks may be subdivided into two classes (Ryu et al. 2003). Merger (or 'internal') shocks are caused by the supersonic motion of infalling substructures, as seen, for example, in Abell 3667 or in the 'bullet cluster' 1E 0657−56 (Markevitch et al. 2002). Typically, the Mach number of these shocks is rather low, $\mathcal{M} \lesssim 3$, (Gabici & Blasi 2003), since the cluster temperature reflects already the depth of the gravitational potential which also determines the maximal velocities in the course of the merger. When the shocks travel outwards into the cluster surroundings, the Mach number increases since the gas there has virtually never been shock-heated and is therefore much colder. Numerical simulations indicate that those accretion (or 'external') shocks reach Mach numbers $\gg$10 (Miniati et al. 2000; Hoeft et al., in preparation; Pfrommer et al. 2006). Basically, clusters are enveloped by a sphere of accretion shocks at a distance, $r_{\rm sh}$, of a few times the virial radius, $r_{\rm vir}$ (Nagai & Kravtsov 2003; Hoeft et al., in preparation). Due to the accretion shock, the temperature of the gas rises from $\sim 10^3$–$10^4$ K to almost the cluster temperature. To obtain a rough estimate for the temperature in the cluster periphery, we utilize the profile given by Loken et al. (2002):

$$T = 1.3\,\langle T\rangle \left(1 + 1.5\,\frac{r}{r_{\rm vir}}\right)^{-1.6},$$

where $\langle T\rangle$ is the emission-weighted temperature of the cluster. With $r_{\rm sh} \sim 3\,r_{\rm vir}$, the temperature in the downstream region of accretion shocks is $\sim$0.09 $\langle T\rangle$. Hence, we can determine the total emission caused by accretion shocks surrounding clusters of galaxies. For a cluster with $\langle T\rangle = 20$ keV and $r_{\rm vir} = 2$ Mpc, we estimate the temperature in the downstream region of the accretion shocks, namely 1.7 keV. Assuming that the electron density at such a large distance from the cluster centre amounts to $10^{-6}\,\mathrm{cm}^{-3}$, we derive the magnetic field by equation (34), and obtain 0.01 μG. With the help of equation (32), we compute the total emission of a sphere with 12 Mpc diameter. We obtain for a strong shock, $\mathcal{M} \gg 10$,

$$\left.\frac{\mathrm{d}P(1.4\,\mathrm{GHz})}{\mathrm{d}\nu}\right|_{\rm acc-sh} \sim 2.2 \times 10^{29}\,\mathrm{erg\,s^{-1}\,Hz^{-1}}.$$

© 2007 The Authors. Journal compilation © 2007 RAS, MNRAS **375,** 77–91

Downloaded from https://academic.oup.com/mnras/article/375/1/77/986307 by guest on 16 August 2022

In reality, the accretion shock geometry is much more complex and projection effects have to be considered. Therefore, a significant fraction of the emission may come from a small region. Note that for such weak magnetic fields the emission region has only a small extension perpendicular to the shock front ($\sim$50 kpc).

Upcoming radio telescopes, such as LOFAR and SKA, will allow us to explore the radio sky with significantly improved sensitivity and resolution in the frequency range from 10 MHz to 1 GHz. Keshet et al. (2004) inferred that the radio emission from structure formation shocks may become detectable with these telescopes. Hence, in the near future we will have much stronger constraints for modelling the relativistic electron populations in clusters of galaxies.

If we assume that 3 per cent of the emission comes from a rather compact region, we expect at 30 MHz a spot-like emission of $\sim 4 \times 10^{29}$ erg s$^{-1}$ Hz$^{-1}$ (note $P \propto \nu^{-s/2}$). If this cluster is located at $z = 0.1$, the flux would amount to 1 mJy. This is close to the sensitivity of LOFAR; hence, accretion shocks with optimal conditions for radio emission will presumably be observed with sensitive radio telescopes in the near future.

## 6 SUMMARY

Galaxy clusters grow either by mergers or by steady accretion, both of which produce large shock fronts. In particular, the extended radio relics (*radio gischt*) in the periphery of clusters are believed to trace these fronts. In analogy to supernova remnants, diffuse shock acceleration may produce a population of relativistic electrons that cool in the downstream region of the shock by IC and synchrotron losses. Here, we compute the total emission in the downstream region per unit area of the shock surface. The resulting analytic expression shows several interesting features: (i) the total spectrum is a power law even if locally the spectrum may steepen towards higher frequencies. The overall slope is close to unity and depends solely on the slope of the initial electron spectrum which, in turn, is directly related to the strength of the shock. Thus, the overall slope of the radio emission may allow us to infer the Mach number of the shock; (ii) the radio emission depends almost like a step-function on the shock strength. For Mach numbers $\lesssim$3, only very little radiation is emitted while for $\mathcal{M} \gtrsim 10$ the emission saturates; (iii) in the regime of weak magnetic fields, $B \ll B_{\rm CMB}$, the total emission is proportional to $B^{1+s/2}$ while for strong magnetic fields the total emission is virtually independent of $B$; and (iv) the width of the emission region, that is, the extension perpendicular to the shock front, has a maximum extension for $B \sim B_{\rm CMB}$.

We analysed the relics in Abell 115, 2256 and 3667 and found that the shocks have Mach numbers in the range of 3 to 5. Weaker shocks would lead to practically no radio emission. Furthermore, we can infer the magnetic fields in the emission regions. We find that for three sample relics the magnetic field is in the range from 0.1 to 0.3 μG. The extension of the relics perpendicular to the shock front serves as an independent indicator for the field strength. The energy fraction stored in the magnetic field seems to be rather low, namely $\xi_B \sim 10^{-3}$.

Assuming that the magnetic field energy density is on average proportional to the thermal one, we derive a radio emission–temperature relation. It agrees strikingly well with that found for radio haloes. Moreover, if in the centres of galaxy clusters, that is, where the radio haloes reside, the magnetic field is about a few μG, the extension of the emission region perpendicular to the shock front would be several hundred kpc. Therefore, it is conceivable that at least part of the halo emission stems from shock waves which swept over the cluster centres within the last 1 Gyr. Using the value obtained for $\xi_B$, we have finally estimated the emission from cosmic accretion shocks. We inferred that at 30 MHz a radio power of $10^{29}$–$10^{30}$ erg s$^{-1}$ Hz$^{-1}$ may be expected from regions where the accretion shock surface is parallel to the line of sight. A detailed computation of the cosmic radio background will be subject of a forthcoming study.

## ACKNOWLEDGMENTS

We gratefully acknowledge support by DFG grant BR 2026/2. We thank Torsten Ensslin for helpful discussions.

## REFERENCES

Amato E., Blasi P., 2005, MNRAS, 364, L76
Ascasibar Y., Sevilla R., Yepes G., Müller V., Gottlöber S., 2006, MNRAS, 371, 193
Axford W. I., Leer E., Skadron G., 1978, 15th International Cosmic Ray Conf. Vol. 11. Bulgarska Akad. na Naukite, Sofia, p. 132
Bell A. R., 1978a, MNRAS, 182, 147
Bell A. R., 1978b, MNRAS, 182, 443
Bennett L., Ellison D. C., 1995, JGR, 100, 3439
Berezhko E. G., Ksenofontov L. T., Völk H. J., 2003, A&A, 412, L11
Blandford R., Eichler D., 1987, Phys. Rep., 154, 1
Blandford R. D., Ostriker J. P., 1978, ApJ, 221, L29
Brunetti G., 2004, J. Korean Astron. Soc., 37, 493
Clarke T. E., Ensslin T., 2006, AJ, 131, 2900
Colafrancesco S., Blasi P., 1998, Astropart. Phys., 9, 227
Dahle H., Kaiser N., Irgens R. J., Lilje P. B., Maddox S. J., 2002, ApJS, 139, 313
Dennison B., 1980, ApJ, 239, L93
Drury L. O., 1983, Rep. Prog. Phys., 46, 973
Dyer K. K., Reynolds S. P., Borkowski K. J., Allen G. E., Petre R., 2001, ApJ, 551, 439
Eke V. R., Navarro J. F., Frenk C. S., 1998, ApJ, 503, 569
Ellison D. C., Cassam-Chenaï G., 2005, ApJ, 632, 920

Downloaded from https://academic.oup.com/mnras/article/375/1/77/986307 by guest on 16 August 2022

Enßlin T. A., Brüggen M., 2002, MNRAS, 331, 1011
Enßlin T. A., Gopal-Krishna, 2001, A&A, 366, 26
Enßlin T. A., Biermann P. L., Klein U., Kohle S., 1998, A&A, 332, 395
Fabian A. C., Reynolds C. S., Taylor G. B., Dunn R. J. H., 2005, MNRAS, 363, 891
Feretti L., 2005, Adv. Space Res., 36, 729
Feretti L., Orrù E., Brunetti G., Giovannini G., Kassim N., Setti G., 2004, A&A, 423, 111
Feretti L., Brunetti G., Giovannini G., Kassim N., Orrú E., Setti G., 2005, J. Korean Astron. Soc., 37, 315
Fujita Y., Sarazin C. L., 2001, ApJ, 563, 660
Gabici S., Blasi P., 2003, ApJ, 583, 695
Giovannini G., Tordi M., Feretti L., 1999, New Astron., 4, 141
Govoni F., Feretti L., 2004, Int. J. Mod. Phys. D, 13, 1549
Govoni F., Enßlin T. A., Feretti L., Giovannini G., 2001a, A&A, 369, 441
Govoni F., Feretti L., Giovannini G., Böhringer H., Reiprich T. H., Murgia M., 2001b, A&A, 376, 803
Govoni F., Markevitch M., Vikhlinin A., VanSpeybroeck L., Feretti L., Giovannini G., 2004, ApJ, 605, 695
Hoeft M., Brüggen M., Yepes G., 2004, MNRAS, 347, 389
Jaffe W. J., 1977, ApJ, 212, 1
Jones F. C., Ellison D. C., 1991, Space Sci. Rev., 58, 259
Kardashev N. S., 1962, SvA, 6, 317
Kempner J. C., Blanton E. L., Clarke T. E., Enßlin T. A., Johnston-Hollitt M., Rudnick L., 2004, in Reiprich T., Kempner J., Soker N., eds, The Riddle of Cooling Flows in Galaxies and Clusters of Galaxies. http://www.astro.virginia.edu/coolflow/proc.php
Keshet U., Waxman E., Loeb A., Springel V., Hernquist L., 2003, ApJ, 585, 128
Keshet U., Waxman E., Loeb A., 2004, ApJ, 617, 281
Levinson A., 1994, ApJ, 426, 327
Loken C., Norman M. L., Nelson E., Burns J., Bryan G. L., Motl P., 2002, ApJ, 579, 571
Malkov M. A., O'C Drury L., 2001, Rep. Prog. Phys., 64, 429
Markevitch M., Gonzalez A. H., David L., Vikhlinin A., Murray S., Forman W., Jones C., Tucker W., 2002, ApJ, 567, L27
Medvedev M. V., Fiore M., Fonseca R. A., Silva L. O., Mori W. B., 2005, ApJ, 618, L75
Medvedev M. V., Silva L. O., Kamionkowski M., 2006, ApJ, 642, L1
Miniati F., Ryu D., Kang H., Jones T. W., Cen R., Ostriker J. P., 2000, ApJ, 542, 608
Miniati F., Jones T. W., Kang H., Ryu D., 2001, ApJ, 562, 233
Nagai D., Kravtsov A. V., 2003, ApJ, 587, 514
Pfrommer C., Springel V., Enßlin T. A., Jubelgas M., 2006, MNRAS, 367, 113
Rephaeli Y., Gruber D., 2003, ApJ, 595, 137
Roettiger K., Burns J. O., Stone J. M., 1999, ApJ, 518, 603
Röttgering H. J. A., Wieringa M. H., Hunstead R. W., Ekers R. D., 1997, MNRAS, 290, 577
Rybicki G. B., Lightman A. P., 1979, in George B. R., Alan P. L., eds, Radiative Processes in Astrophysics. Wiley-Interscience, New York, p. 400
Ryu D., Kang H., Hallman E., Jones T. W., 2003, ApJ, 593, 599
Sarazin C. L., 1999, ApJ, 520, 529
Shibata R., Honda H., Ishida M., Ohashi T., Yamashita K., 1999, ApJ, 524, 603
Slee O. B., Roy A. L., Murgia M., Andernach H., Ehle M., 2001, AJ, 122, 1172
Sun M., Murray S. S., Markevitch M., Vikhlinin A., 2002, ApJ, 565, 867
Vikhlinin A. A., Markevitch M. L., 2002, Astron. Lett., 28, 495
Vink J., Laming J. M., 2003, ApJ, 584, 758
Wentzel D. G., 1974, ARA&A, 12, 71

This paper has been typeset from a TEX/LATEX file prepared by the author.

Downloaded from https://academic.oup.com/mnras/article/375/1/77/986307 by guest on 16 August 2022